

Supporting Information for

Biopolymer-reinforced synthetic granular nanocomposites for affordable point-of-use water purification

Mohan Udhaya Sankar^{a,1}, Sahaja Aigal^{a,1}, Shihabudheen M. Maliyekkal^{a,1}, Amrita Chaudhary^a, Anshup^a, Avula Anil Kumar^a, Kamalesh Chaudhari^a and Thalappil Pradeep^{a,2}

^aDST Unit of Nanoscience (DST UNS) and Thematic Unit of Excellence,
Department of Chemistry, Indian Institute of Technology Madras,
Chennai 600 036, India.

²Correspondence and requests for composites should be addressed to T.P. (pradeep@iitm.ac.in)

Supporting Information	Title	Page No.
SI	Methods	3
SI	Material characterization	3

Supporting Figure	Title	Page No.
S1.	Transmission electron micrograph and EDAX elemental mapping of Ag-BM	5
S2.	Performance trials for gravity-fed water purifier device containing Ag-BM as water purification composite	6
S3.	Silver ion leaching as a function of temperature	7
S4.	X-ray diffraction pattern of BM and Ag-BM	8
S5.	Field emission scanning electron microscopic image of Ag-BM	9

S6.	XPS survey spectra of Ag-BM	10
S7.	SEM-EDAX elemental spectrum and elemental imaging	11
S8.	AFM images of surface roughness of Ag-BM	12
S9.	Effect of water quality on performance of Ag-BM	13
S10.	Effect of variations in input water quality on antibacterial performance of Ag-BM	14
S11.	Effect of water quality used for reactivation of Ag-BM	15
S12.	Antibacterial performance for Ag-BM reactivation by alternate methods	16
S13.	Antiviral performance trials for Ag-BM in batch	17
S14.	Hyperspectral imaging of <i>E. coli</i>	18
S15.	Hyperspectral imaging of silver nanoparticles	19
S16.	Analysis of aluminium and TOC leaching	20
S17.	Fluorescence microscopy images of treated bacteria	21
S18.	Cyst removal performance tested with 4-6 micron polystyrene spheres	22
S19.	Direct shear test (horizontal shear stress vs. horizontal displacement)	23
S20.	Mohr-coulomb failure pattern (shear stress vs. normal stress)	24

Supporting Table	Title	Page No.
S1.	Physicochemical characteristics of influent natural drinking water	25

SI Methods

Fluorescence microscopy protocol: 1L of 10^6 CFU/mL *E. coli* containing water was contacted with Ag-BM for an hour and it was repeatedly centrifuged at 20,000 rpm to obtain a bacterial pellet. This pellet was resuspended in 1 mL of 0.85% saline to obtain a final bacterial concentration of 10^9 CFU/mL. Staining was done according to Invitrogen Molecular Probes protocol. Briefly, 3 μ L of a fluorescent probe mixture containing 3.34 μ M green fluorescent nucleic acid stain SYTO 9 and 15 μ M red fluorescent nucleic acid stain PI was combined with 1 mL of bacterial suspension. The mixture was incubated in dark for 15 min at room temperature and a 5 μ L aliquot was placed on a glass slide, which was then covered by a cover slip, sealed and examined under Fluorescence microscope. Excitation was done for SYTO 9 at 465-495 nm and at 530-560 nm for PI. Emission was collected using a band pass filter for SYTO 9 at 515-555 nm and a long pass filter for PI at 590 nm.

Mechanical testing of composite: The shear strength of the media was measured at dry and wet conditions, separately. Around \sim 140 g of granular media was packed in a 6 cm x 6 cm x 6 cm (LxBxH) sample holder and horizontal shear stress was measured under normal stress of 50, 100 and 200 kPa.

SI Material characterization

The identification of the phase(s) of the as-prepared sample was carried out by X-ray powder diffraction (Bruker AXS, D8 Discover, USA) using Cu-K α radiation at $\lambda = 1.5418$ Å. Surface morphology, elemental analysis and elemental mapping studies were carried out using a Scanning Electron Microscope (SEM) equipped with Energy Dispersive Analysis of X-rays (EDAX) (FEI Quanta 200). Field Emission SEM measurements were done with FEI Nova NanoSEM 600 instrument. High Resolution Transmission Electron Microscopy (HRTEM) images of the sample were obtained with JEM 3010 (JEOL, Japan) operating at 300 keV. Elemental mapping was done with a TEM EDAX. X-ray Photoelectron Spectroscopy (XPS) measurements were done using

ESCA Probe TPD of Omicron Nanotechnology. Polychromatic Mg K α was used as the X-ray source ($h\nu = 1253.6$ eV). Binding energy was calibrated with respect to C 1s at 284.5 eV. Total silver, arsenic and lead concentrations in water were estimated using inductively coupled plasma mass spectrometry (ICP-MS) (Agilent Technologies, 7700x ICP-MS and PerkinElmer NexION 300 ICP-MS). Atomic Force Microscopy (AFM) measurements were done using a Witec GmbH confocal Raman microscope (CRM-Alpha300 S). Bacteria treated with silver nanoparticles and those treated with Ag-BM, were viewed under the Cytoviva microscope, attached to a Hyperspectral imaging (HSI) system. The system captures the VNIR (400-1000 nm) spectrum within each pixel of the scanned field of view. The bacteria were treated for a period of 2 h, and 2 μ L of the same were spotted on glass slides. The spotted samples were allowed to dry for over 4 h before imaging. Imaging was done at 100x magnification, using a halogen lamp (400-1000 nm) as the light source. Nikon ECLIPSE 80i fluorescence microscope was used to image stained bacteria.

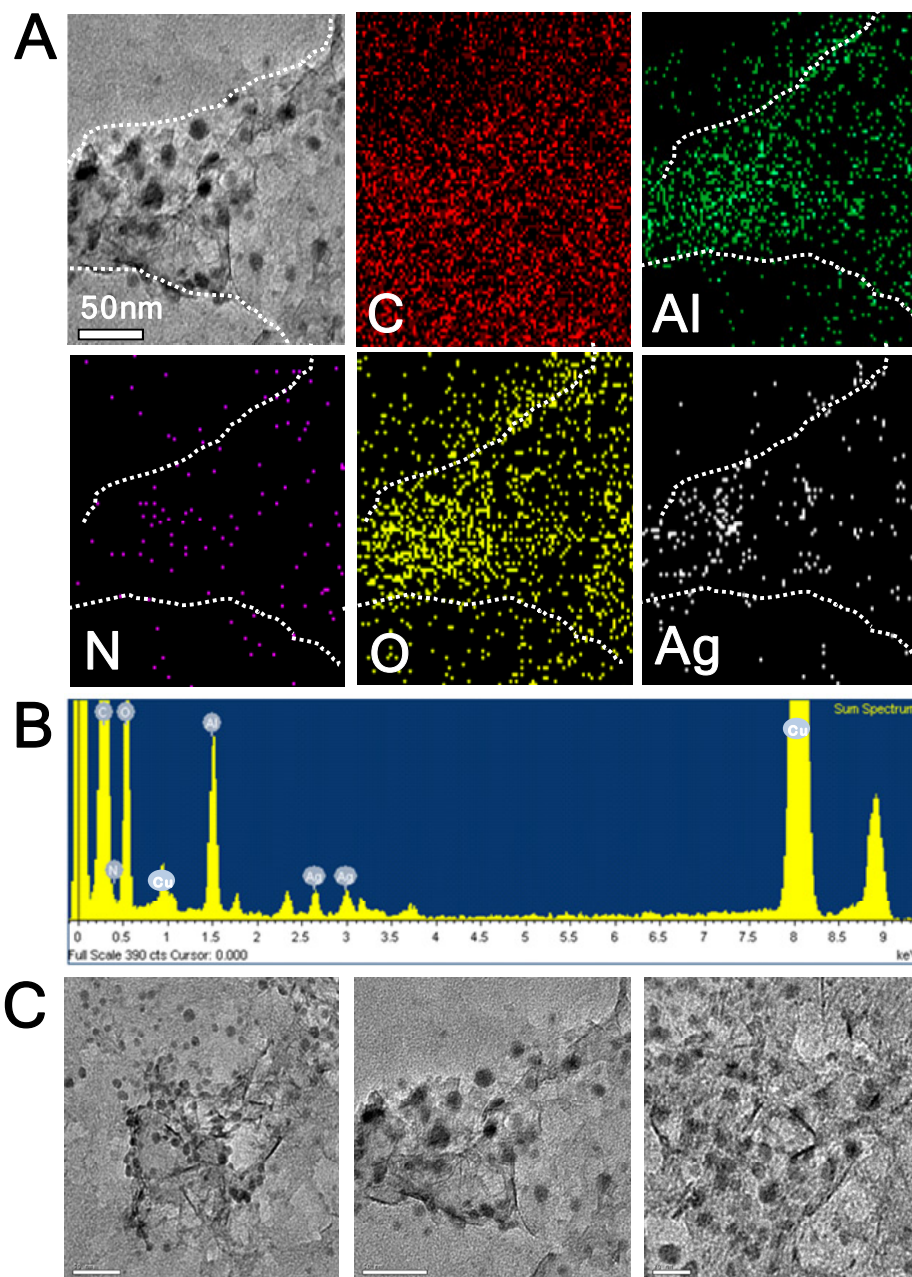


Fig. S1. Transmission electron micrograph and EDAX elemental mapping of Ag-BM. (A) EDAX elemental imaging of Ag-BM. Top extreme left is the TEM image and others are elemental maps from the region. **(B)** EDAX spectrum of **(A)** confirming the presence Ag. **(C)** HRTEM micrographs of Ag-BM (Scale bar is 50 nm). The uniform carbon image is due to the grid and the material. Al and O are present uniformly due to AlOOH and their pattern resembles the pattern of the sample (marked). Ag is also present in this region. The spatial resolution of EDAX resolution is good enough to see isolated particles. The Cu lines are due to the grid used.

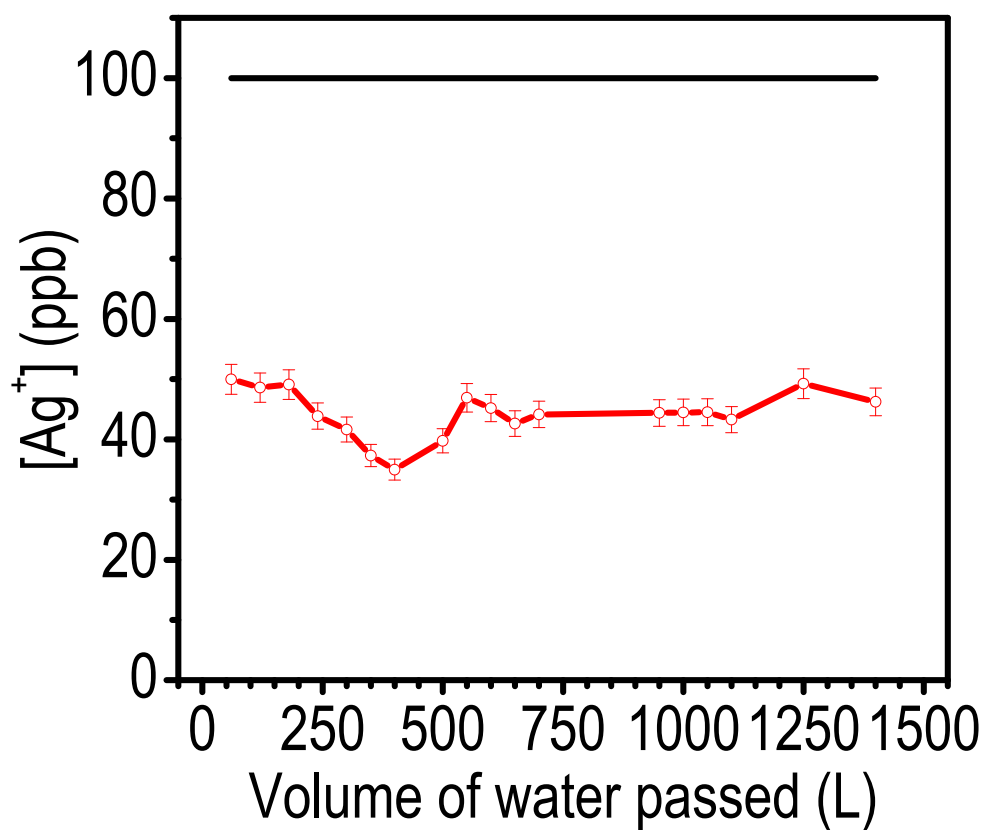


Fig. S2. Performance trials for gravity-fed water purifier device containing Ag-BM as the water purification composite. Analysis of silver ion concentration in output water measured by ICP-MS (red) in cartridge study (refer: *Materials and Methods*). The permissible limit for silver ion concentration in drinking water is shown as black line. Cartridge was run for 1500 L without any reactivation.

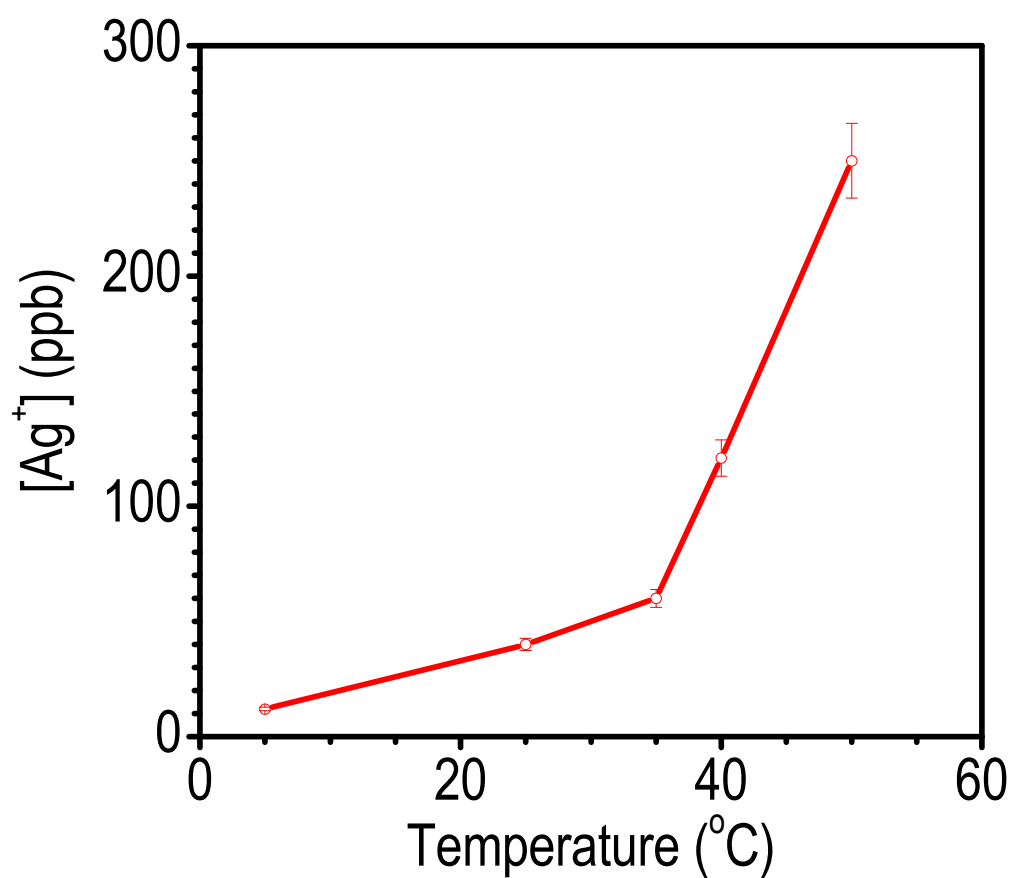


Fig. S3. Silver ion leaching as a function of temperature. Silver ion leaching from Ag-BM in water at temperatures of 5, 25, 35, 40 and 50 °C (measured using ICP-MS). The amount of silver ions leached in water at RT (25-35 °C) is 40 ± 10 ppb, when trials were done in batch.

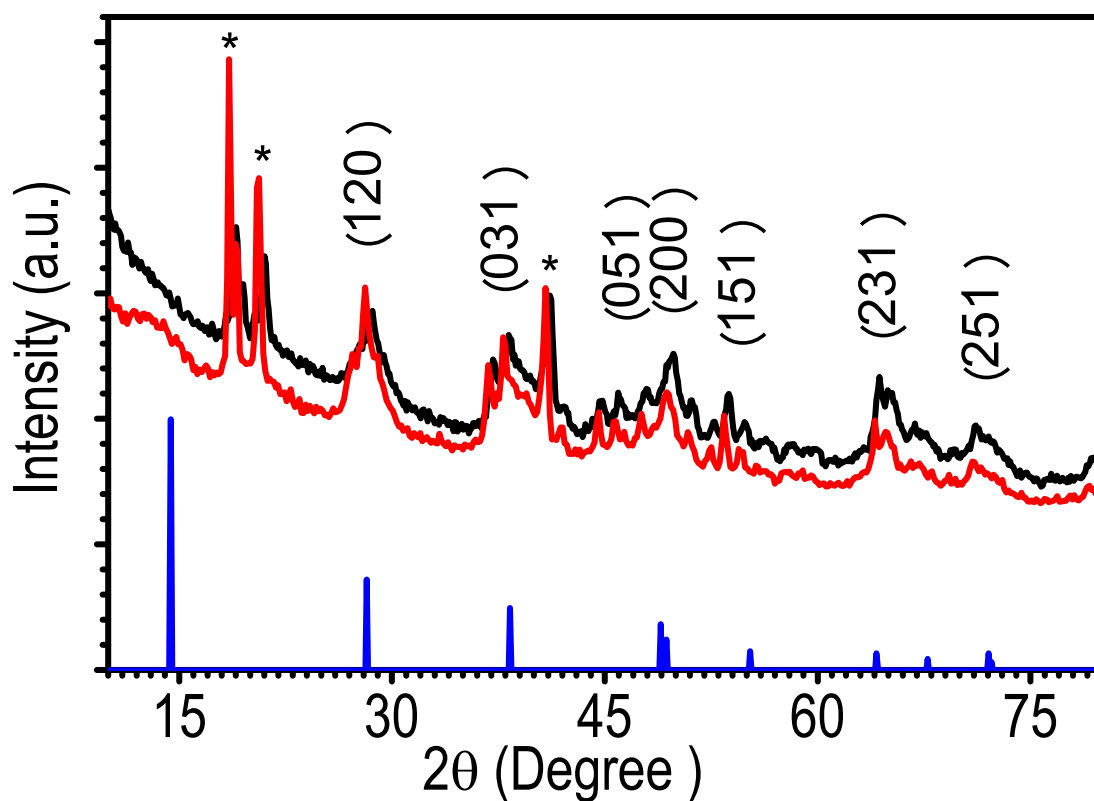


Fig. S4. X-ray diffraction patterns of BM and Ag-BM. XRD patterns of BM (black) and Ag-BM (red). BM showed peaks corresponding to (120), (013), (051), (151), (200), (231) and (251) planes. All these peaks can be indexed to orthorhombic-AIOOH shown in blue colour (JCPDS # 83-2384). The broadened XRD peaks imply that the crystallite size of BM particles is very small. The mean crystallite size calculated from the Scherrer formula shows that AIOOH nanocrystals are of an average size of 3.5 nm. The presence of organic template (chitosan) is also clear from the XRD data. The peaks marked by * corresponding to 2θ (in degrees) = 18.7° , 20.6° and 41.2° are attributed to the presence of the organic template. There is a definite difference in the full-width at half maxima (FWHM) for the peaks corresponding to AIOOH and organic template. Addition of Ag to BM doesn't lead to new diffraction features, presumably due to low concentration of Ag.

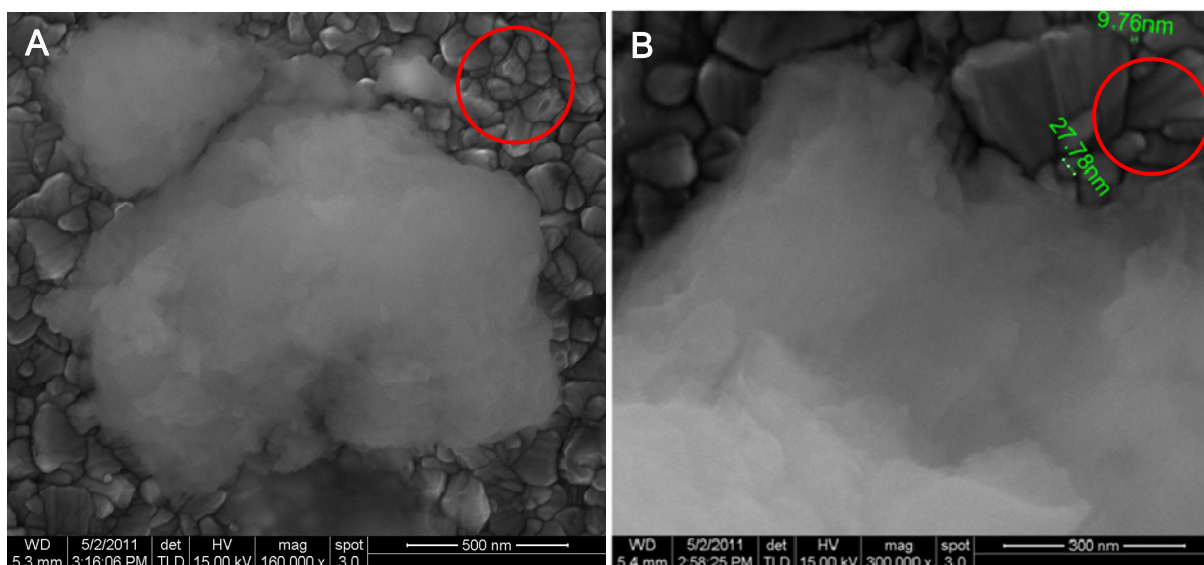


Fig. S5. Field emission scanning electron microscopic image of Ag-BM. FESEM images of an Ag-BM grain at two magnifications. Silver nanoparticles are not seen on the surface of the BM composite, although the substrate particles (ITO, indium tin oxide) in similar size range (10-30 nm) are clearly visible. A part of the ITO coated glass substrate is highlighted by the red circle to illustrate this point. This indicates that silver nanoparticles are embedded and well protected in the BM matrix.

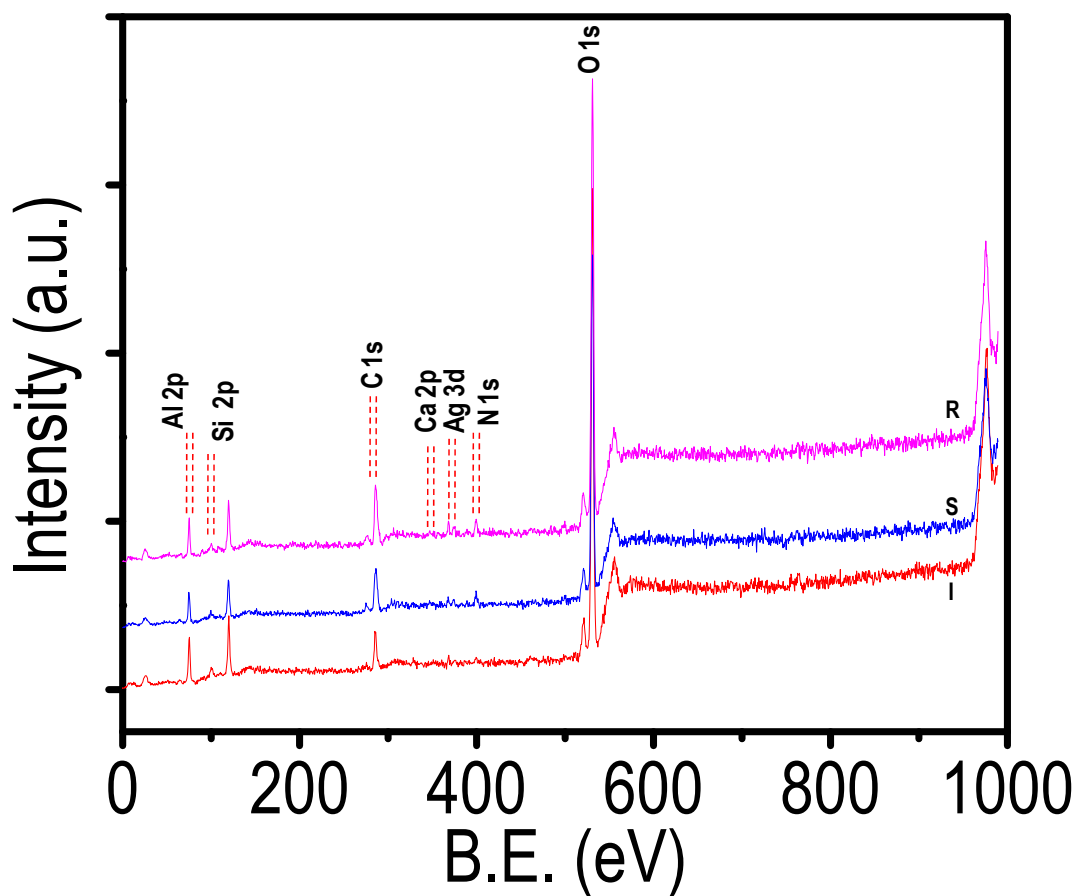


Fig. S6. XPS survey spectra of Ag-BM. XPS survey spectra of Ag-BM samples (I) Prior to use, (S) upon saturation of anti-bacterial activity and (R) upon reactivation in distilled water at 70 °C. The spectra are essentially the same except in Ca 2p and Si 2p regions, which are marked. N 1s is also present in I, although with reduced intensity.

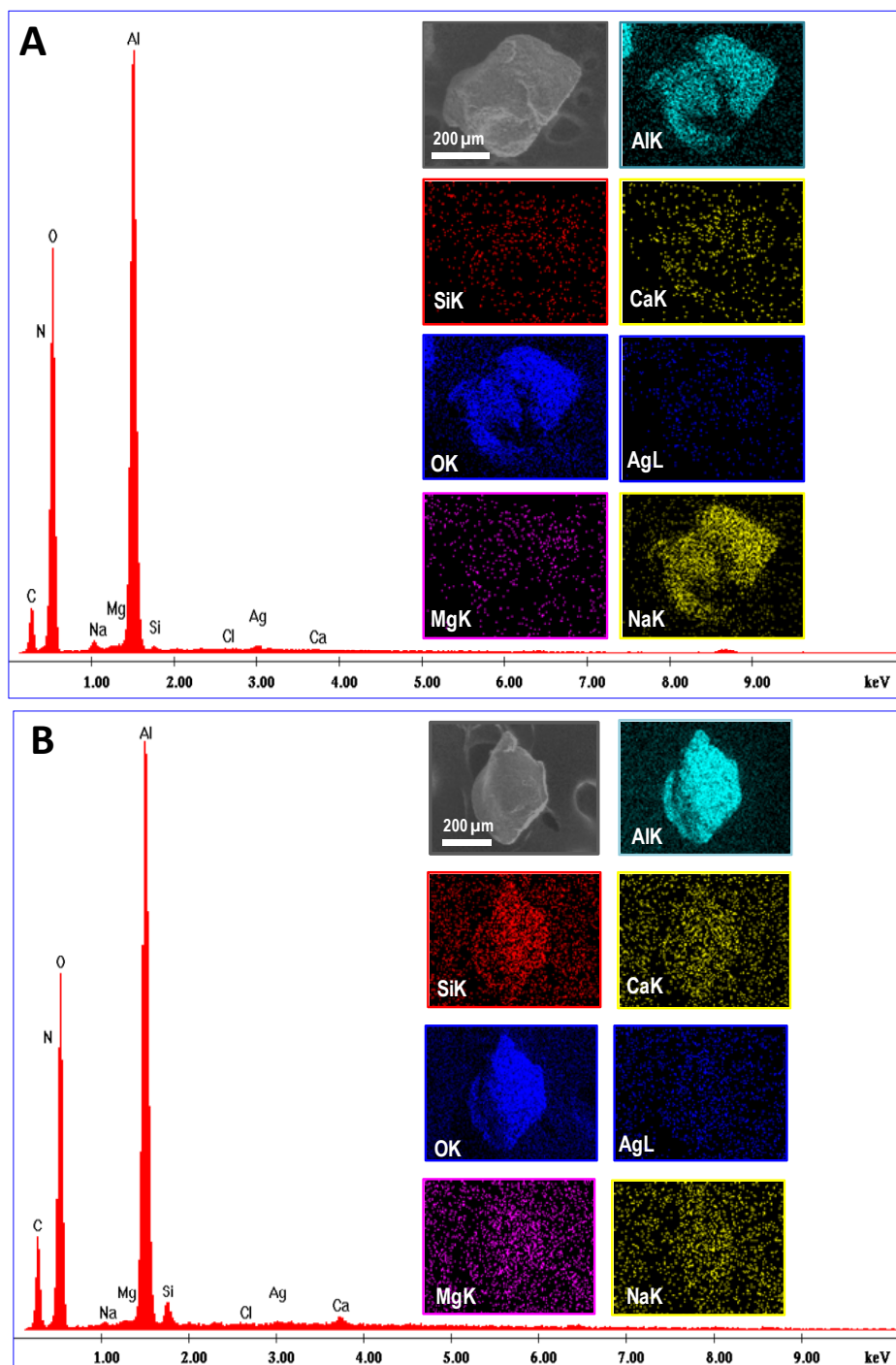


Fig. S7. SEM-EDAX elemental spectrum and elemental imaging. SEM-EDAX of **(A)** freshly prepared Ag-BM and **(B)** saturated Ag-BM. Natural drinking water (without treatment so that there is a residual bacterial count in it) was used for testing. Presence of deposits containing Ca and Si is seen on the saturated Ag-BM material.

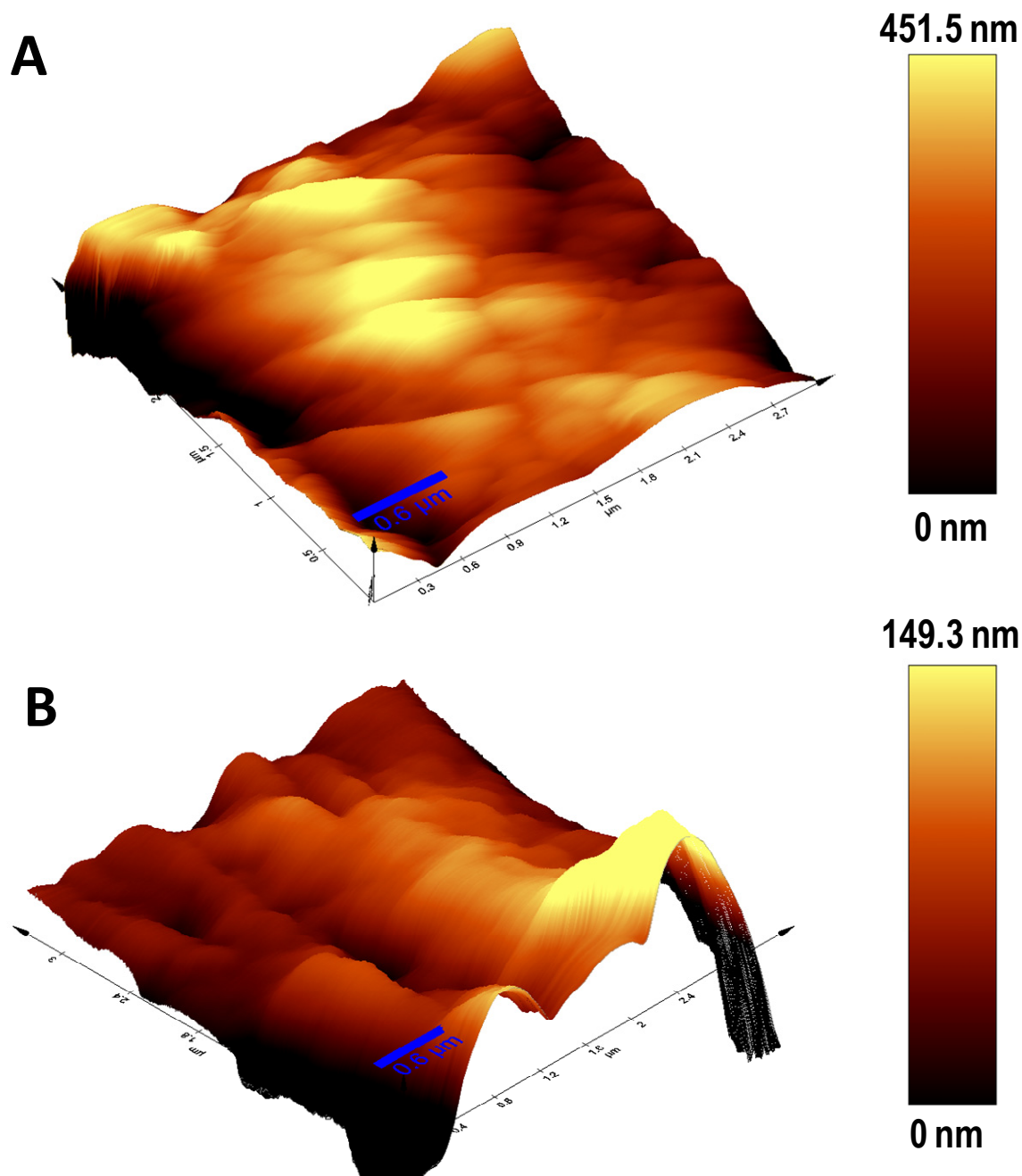


Fig. S8. AFM images of surface roughness of Ag-BM. 3D AFM images of surface roughness of (A) initial Ag-BM and (B) saturated Ag-BM. The high profile is also shown. Increased inhomogeneity, possibly due to deposits is seen in B.

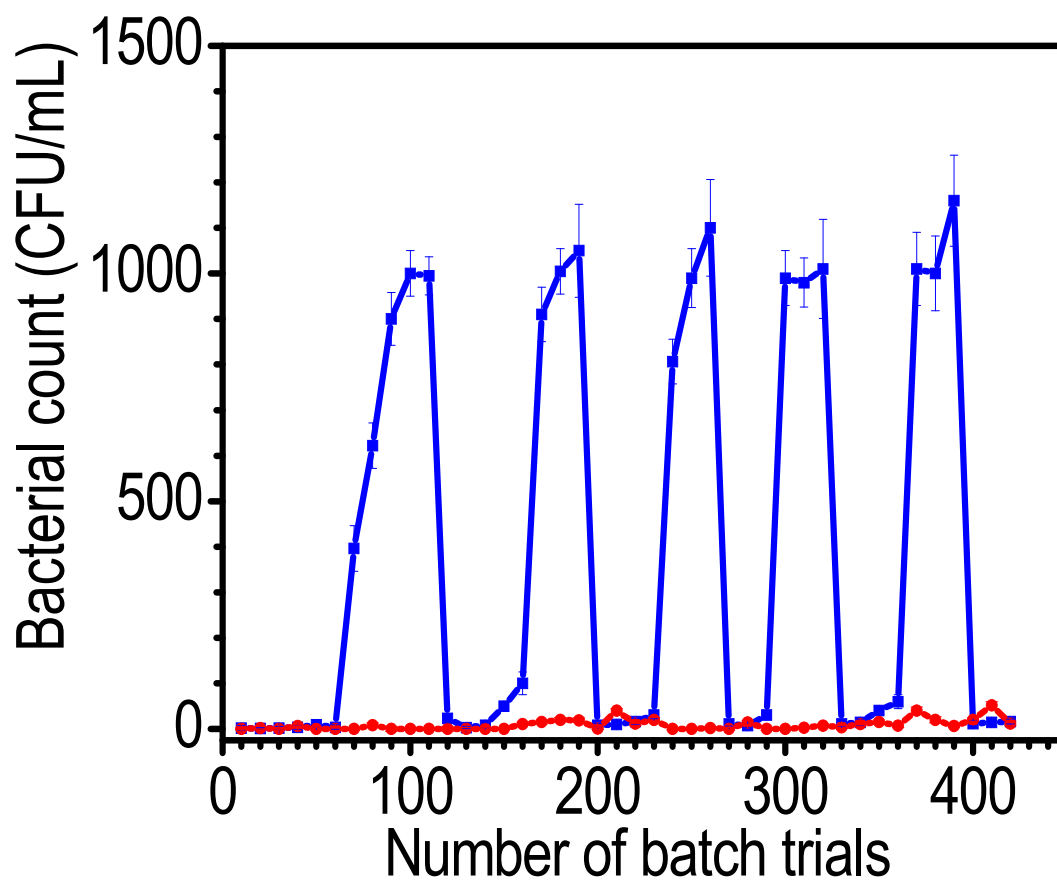


Fig. S9. Effect of water quality on performance of Ag-BM. Performance comparison for Ag-BM shaken in tap water (blue trace) and ultrapure water (red trace). The antibacterial efficacy of the composite in ultrapure water is due to the absence of interfering species typically found in tap water. As in other batch experiments, 2g of the composite was shaken in 100 mL of ultrapure water spiked with 0.85% NaCl (to avoid osmotic rupture) and bacterial input load of 10^5 CFU/mL and the solution was plated after 1 h. The composite works indefinitely without the need for reactivation.

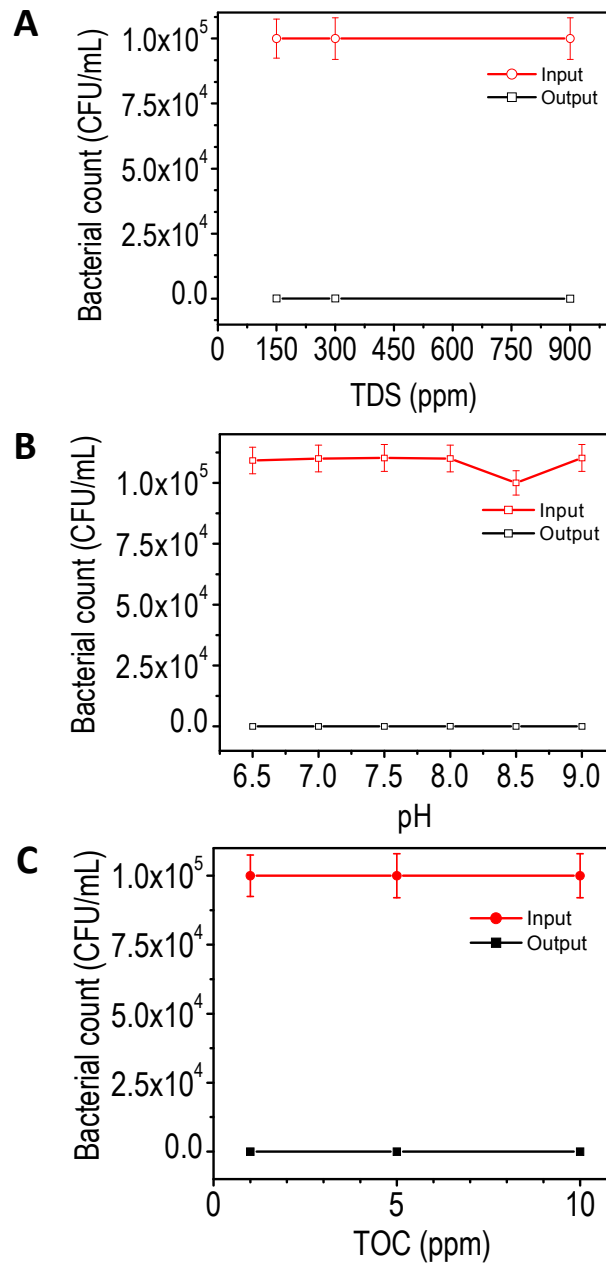


Fig. S10. Effect of variations in input water quality on antibacterial performance of Ag-BM.

Performance of Ag-BM against *E. coli* was tested in batch, by varying **(A)** the ionic strength of synthetic challenge water (pH held constant at 7.0 ± 0.2), **(B)** pH of the synthetic challenge water (TDS held constant at 300 ppm) and **(C)** the organic (humic acid) content of the synthetic challenge water (pH and TDS held constant at 7.0 ± 0.2 and TDS 300 ppm, respectively). The average input concentration was 1×10^5 CFU/mL. Activity of the composite does not diminish with variation in TDS, pH as well as TOC of synthetic challenge water.

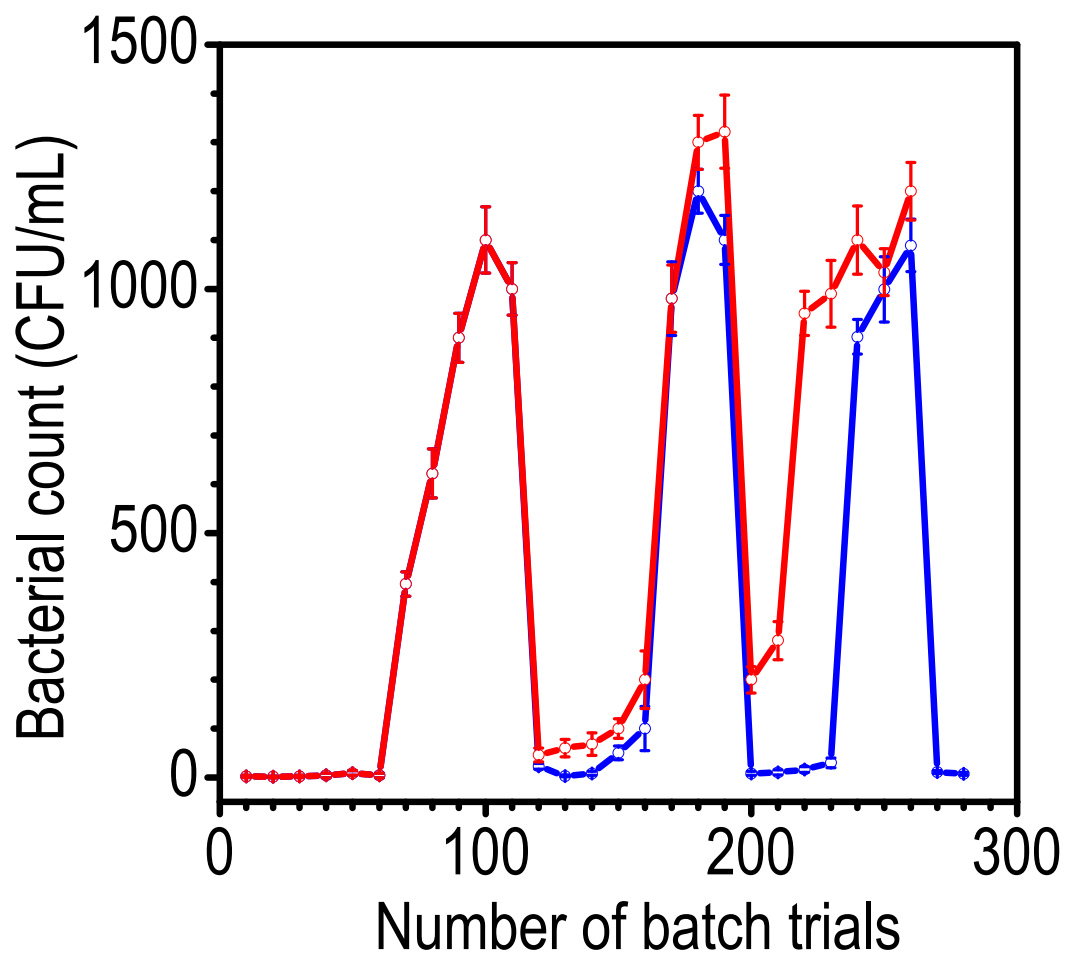


Fig. S11. Effect of water quality used for reactivation of Ag-BM. Performance comparison for Ag-BM reactivated with distilled water (blue trace) and tap water (red trace) at 70 °C. Unlike reactivation of composite in tap water, reactivation in distilled water leads to nearly complete recovery of anti-bacterial performance (output count came to zero). The composite exhibits only 2 cycles of reactivation before getting exhausted in tap water. On the contrary, the composite can be reactivated for at least 5 cycles, if reactivation is conducted in distilled or quality drinking water.

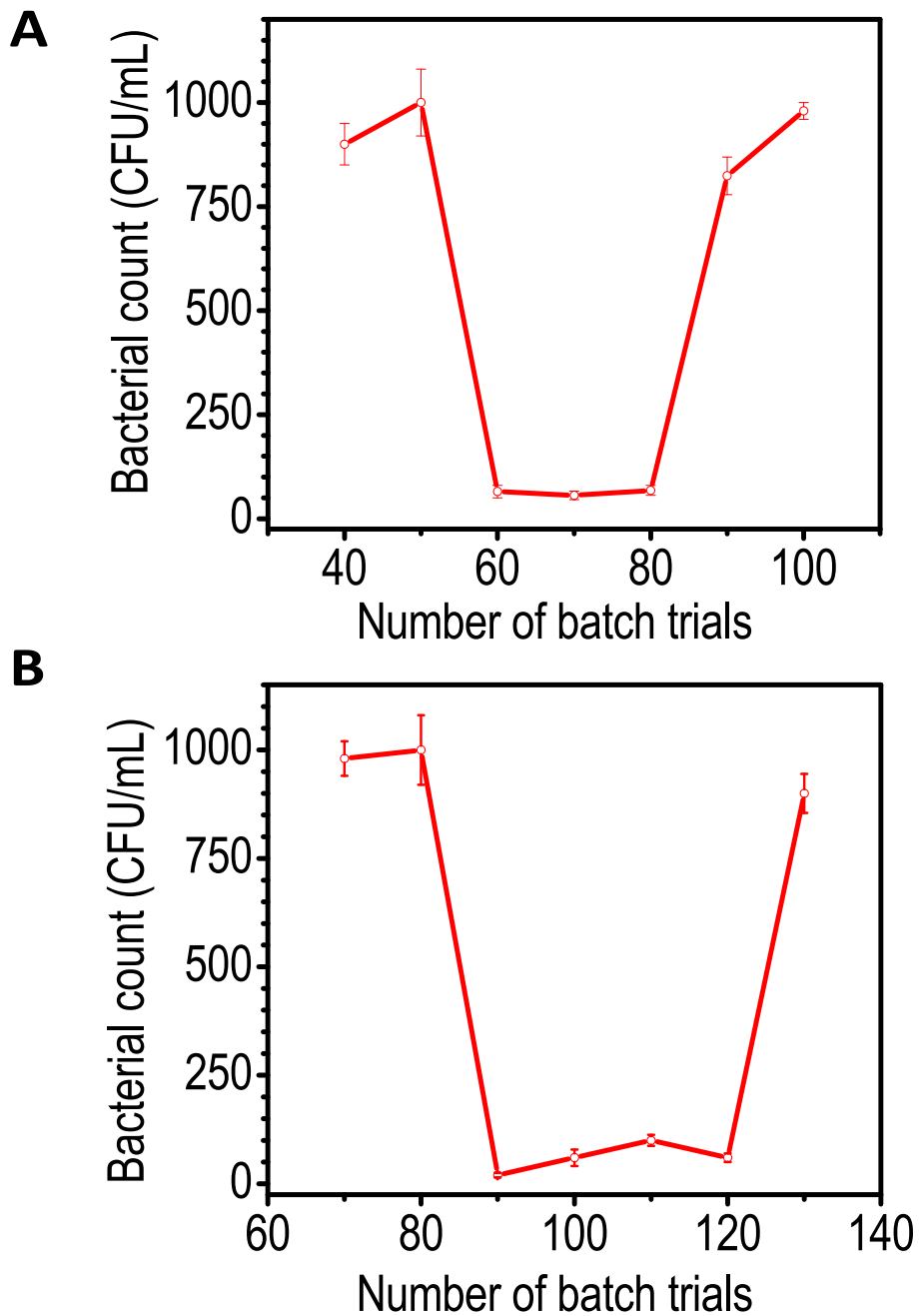


Fig. S12. Antibacterial performance for Ag-BM reactivation by alternate methods. Reactivation using **(A)** citric acid (10 mM) (alternatively, 4 drops of fresh lemon juice is used, pH 5.5 ± 0.5) and **(B)** hydrogen peroxide (100 ppm). It is evident that chemical methods of reactivation are equally efficient in recovering the performance of the composite.

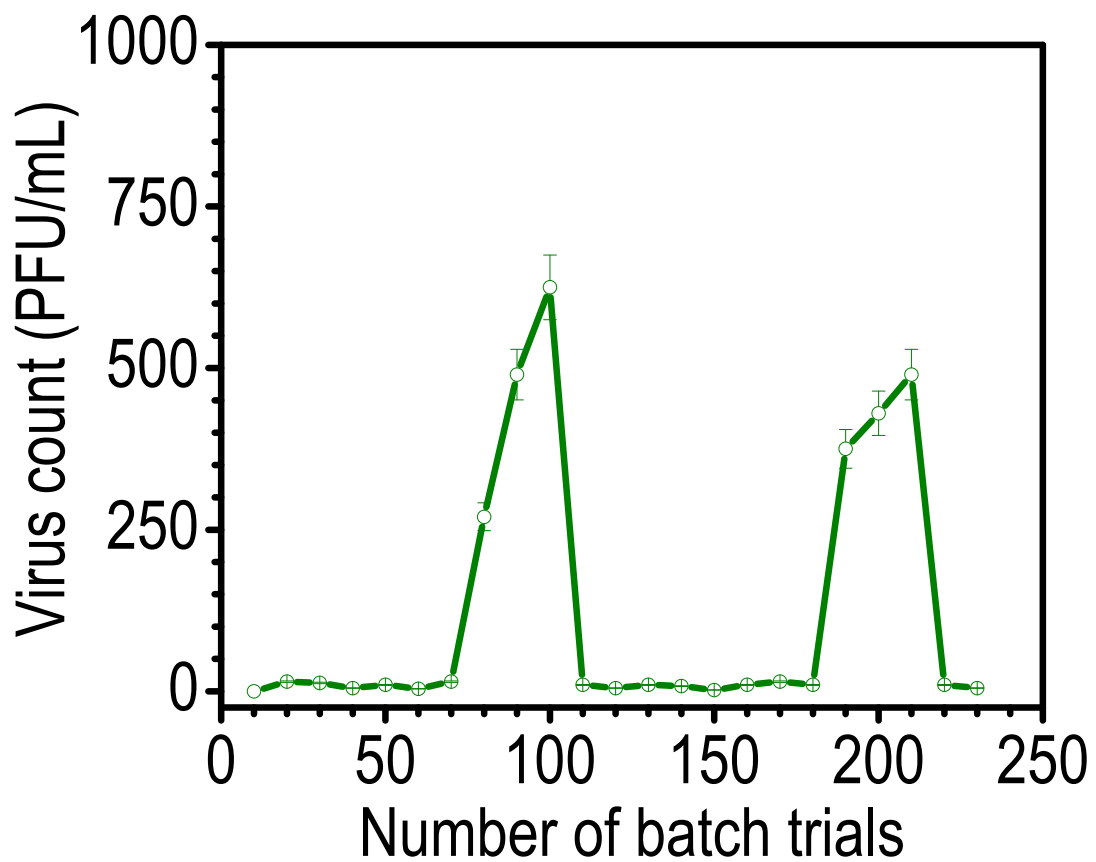


Fig. S13. Antiviral performance trials of Ag-BM in batch. Performance of Ag-BM against MS2 bacteriophage was tested in batch. The average input concentration was 1000 PFU/mL. The composite was reactivated after the 3 consecutive saturation points (trial numbers 80-100 and 190-210) were obtained. The antiviral performance is comparable to antibacterial performance as the composite regains its property after reactivation.

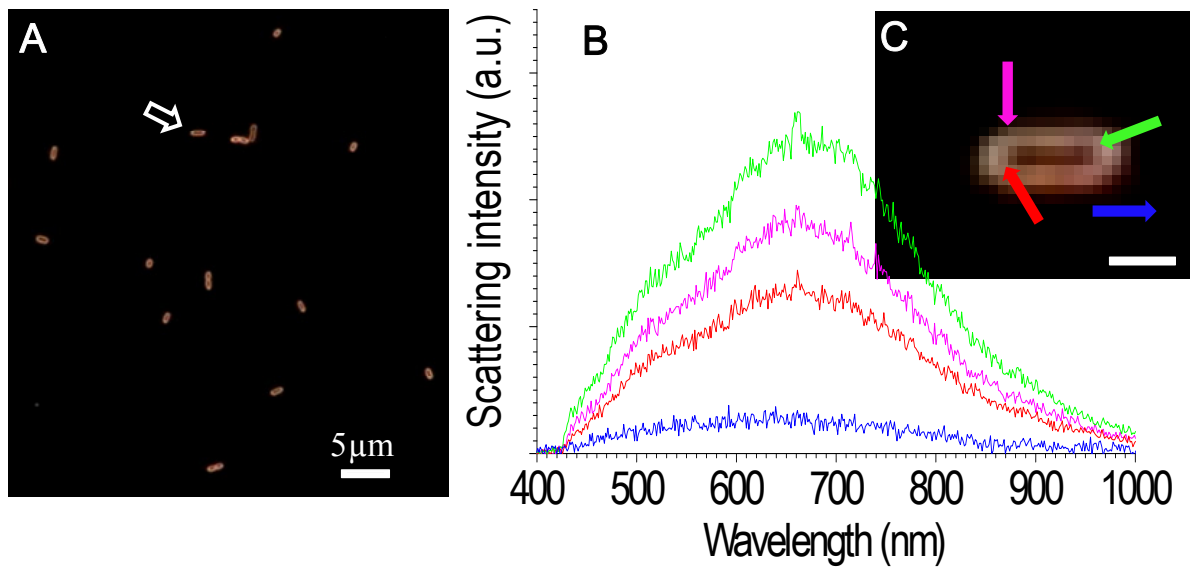


Fig. S14. Hyperspectral imaging of *E. coli*. (A) Hyperspectral image of *E. coli*, (B) spectra collected at various borders of *E. coli* and (C) expanded hyperspectral image of *E. coli* used for collection of spectra. The scale bar is 1 μm. The spectrum essentially resembles the lamp spectrum as there are no absorbing species in a bacterium.

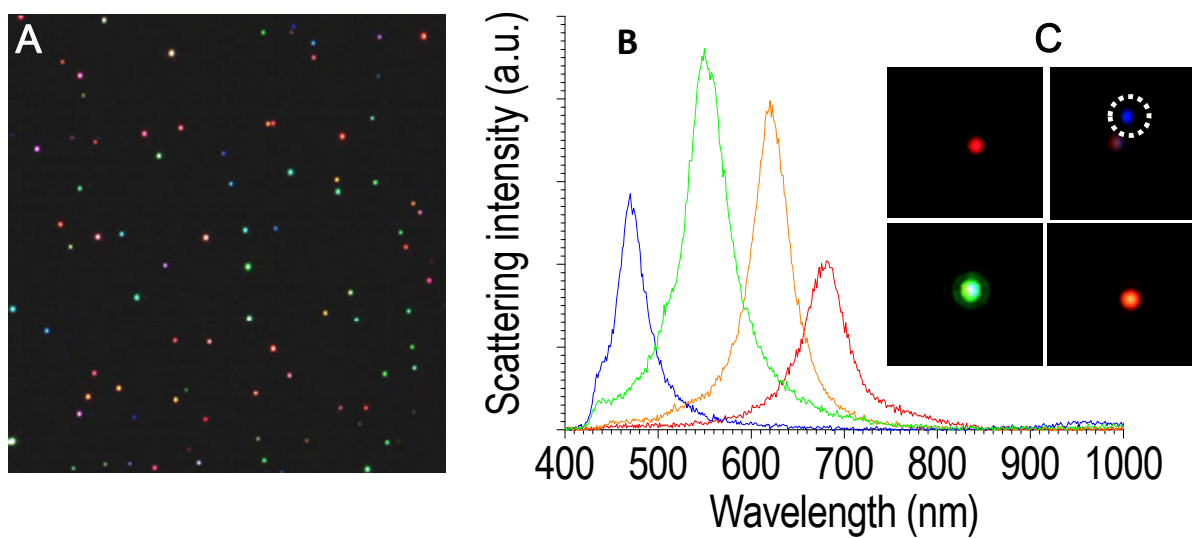


Fig. S15. Hyperspectral imaging (HSI) of silver nanoparticles. HSI images of **(A)** nanoparticles in water, **(B)** spectra collected for single nanoparticles showing different colors due to differences in absorption maxima and **(C)** zoomed images of the corresponding nanoparticles.

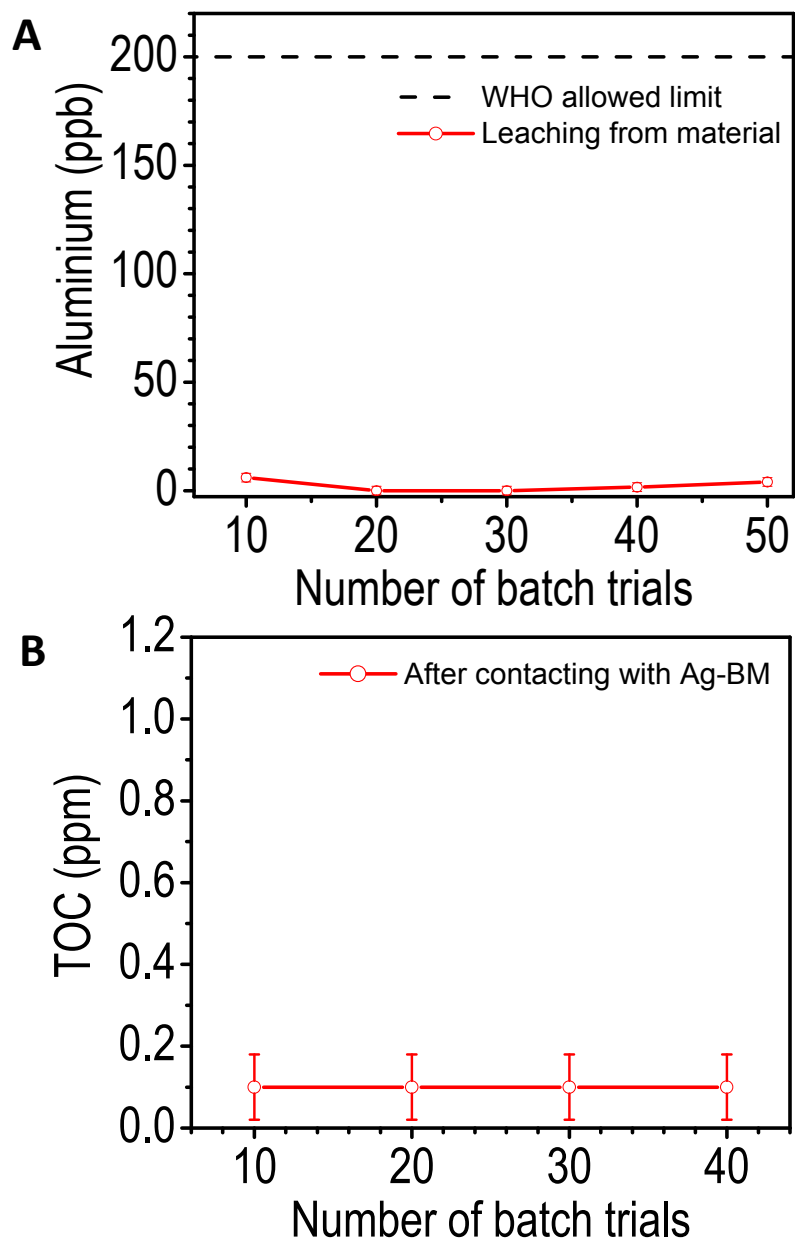


Fig. S16. Analysis of aluminium and TOC leaching. **(A)** Analysis of aluminum concentration in output water measured by ICP-MS (red) in batch trials. The maximum permissible limit for aluminum ion concentration in drinking water is shown as red line. **(B)** Analysis of leached total organic carbon (TOC) in output water. The limit of detection of TOC measurement was estimated to be 80 ppb.

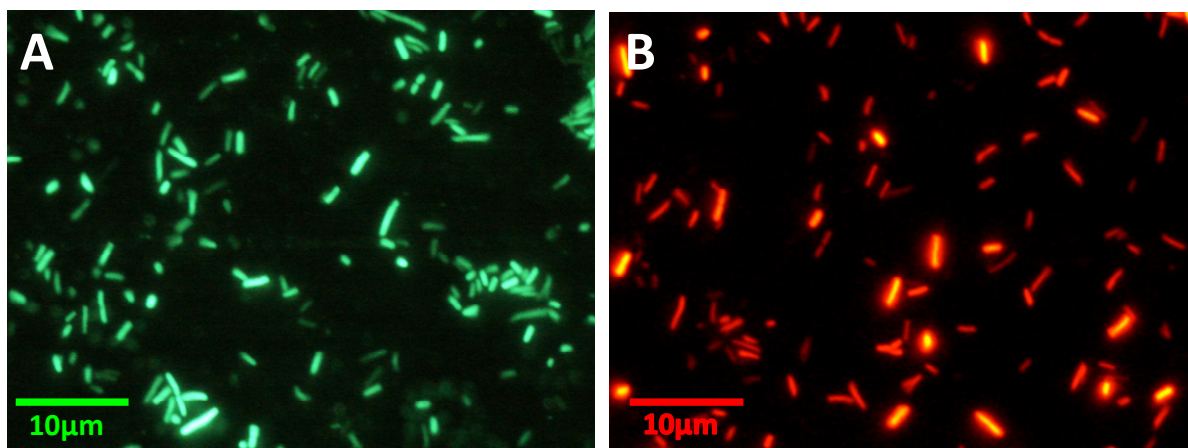


Fig. S17. Fluorescence microscopy study of treated bacteria. Fluorescence microscopy images of bacteria (*E. coli*) after staining with SYTO 9 (green) and PI (red). **(A)** Untreated and **(B)** treated with Ag-BM composite for 1h. Each image is a result of superposition of an image taken for the green fluorescent dye and red fluorescent dye using the appropriate filters. The scale bar is 10 μm . Fluorescence microscopy study supports that bacteria are killed within 1h after treating with Ag-BM.

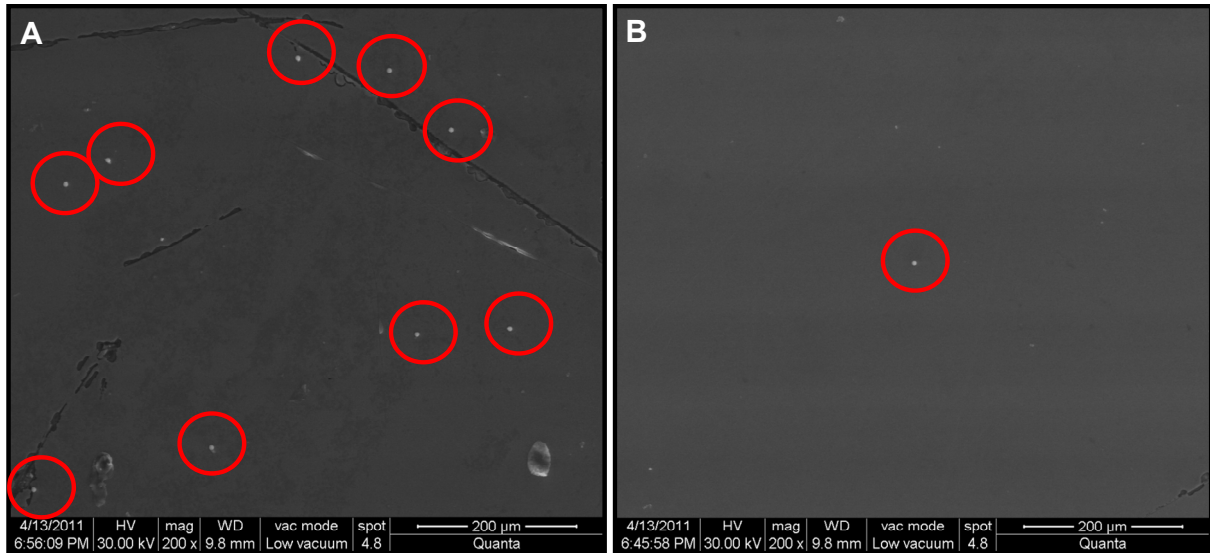


Fig. S18. Cyst removal performance tested with 4-6 micron polystyrene spheres. SEM images of 4-6 micron polystyrene spheres. **(A)** Input count: 10^6 particles/L and **(B)** output count: 1 particle is seen in the 1000 times concentrated sample (<3 particles/L). The input water containing polystyrene spheres was passed through the porous carbon block as per NSF P231 protocol (polystyrene spheres are used as representative for cyst, in terms of size) and removal capacity is higher than 5 log. The porous carbon block removes cysts through physical filtration.

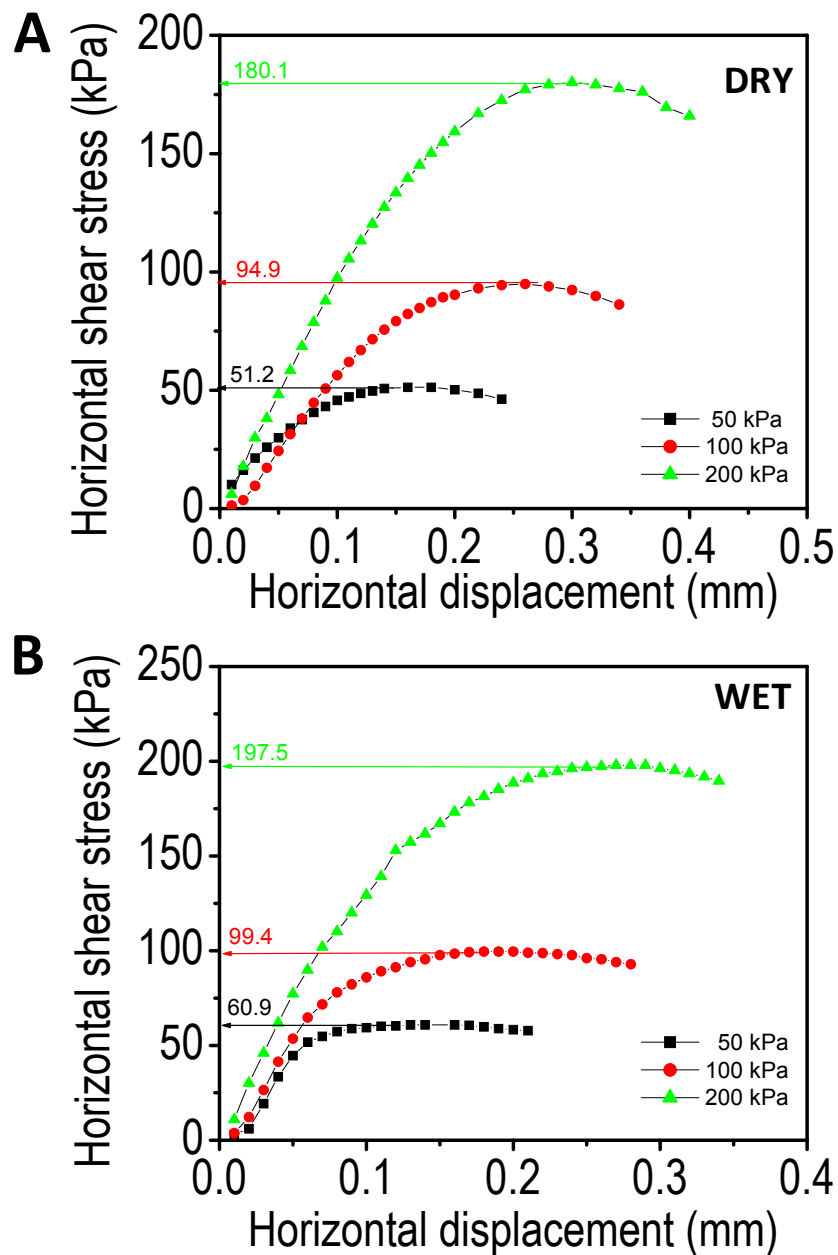


Fig. S19. Direct shear test (Horizontal shear stress vs. Horizontal displacement). Plot of horizontal shear stress vs. horizontal displacement of loosely packed media obtained from direct shear tests: **(A)** measured at dry condition and **(B)** measured at wet condition.

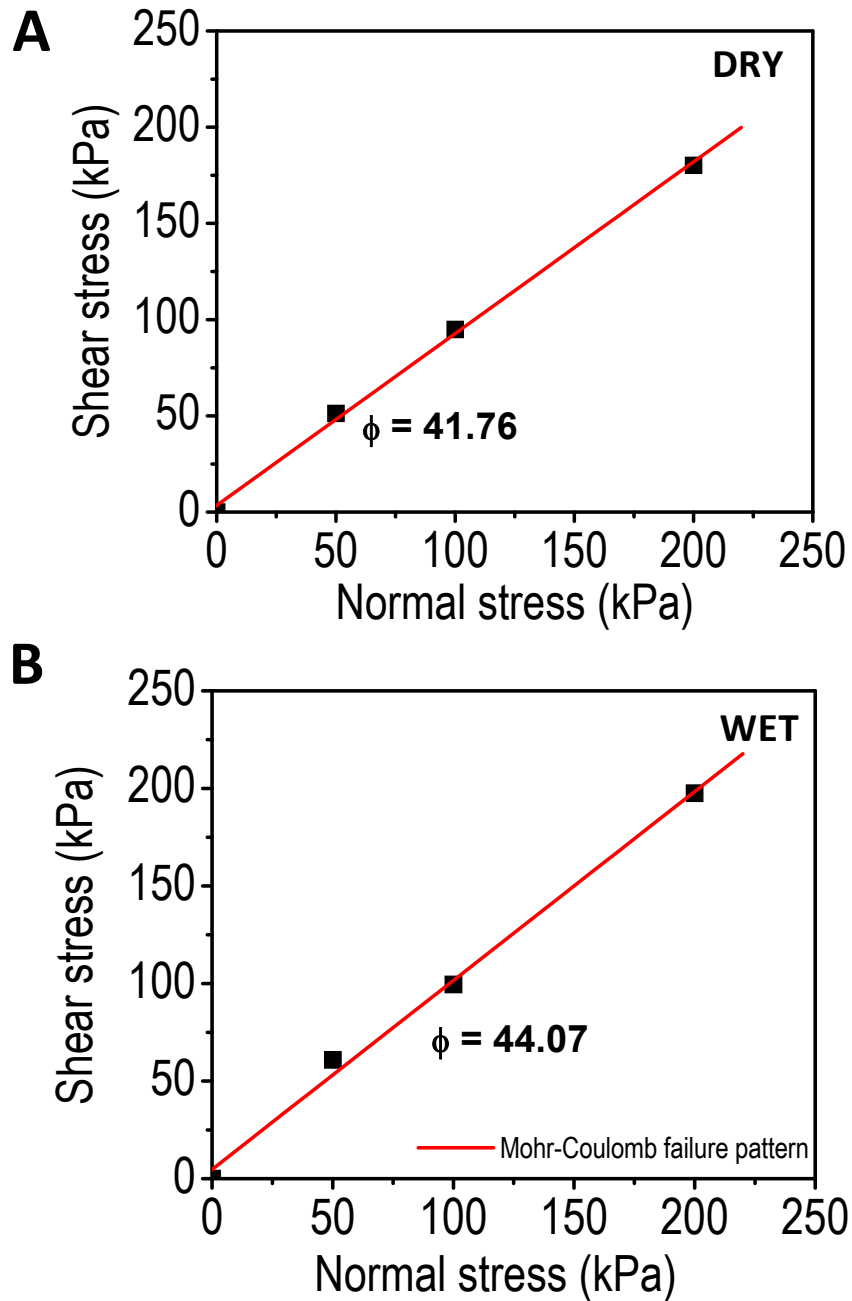


Fig. S20. Mohr-Coulomb failure pattern (Shear stress vs. Normal stress). Plot of shear stress vs. normal stress of loosely packed media showing the straight-line approximation of the Mohr-Coulomb failure pattern: **(A)** measured at dry condition and **(B)** measured at wet condition.

SUPPORTING TABLE

Table S1. Physicochemical characteristics of influent natural drinking water

(Note: All parameters are expressed in mg L⁻¹, except for pH and conductivity)

Parameters	Value
Total coliforms (CFU/mL)	1-2 x 10 ³
p H @25°C	7.8
Conductivity (µS/cm)	640.000
Fluoride	0.573
Chloride	86.340
Nitrate	1.837
Sulphate	32.410
Silicate	15.870
Lithium	ND
Sodium	53.740
Ammonium	ND
Potassium	2.330
Magnesium	14.340
Calcium	28.720

ND-not detected

Natural drinking water (without treatment so that there is a residual bacterial count in it) was used for testing to ensure that that the material functions in the field.